Progress In Electromagnetics Research M, Vol. 60, 57–65, 2017

Horn Antenna Generating Electromagnetic Field with Orbital Angular Momentum

Min Huang*, Xianzheng Zong, and Zaiping Nie

Abstract—A novel method for generating electromagnetic field with orbital angular momentum (OAM) and correspondingly a practical design based on conical horn antenna are proposed in this paper. The OAM modes of $\pm m$ for r/φ field components and $\pm(m-1)$ for x/y ones can be generated by superposing the two orthogonal polarization degenerate TE_{mn} modes in circular waveguide through a mode-transformation section, and then radiated from the horn in the far end. The effectiveness of the proposed method is analyzed from physical mechanisms and demonstrated by both simulation and experiment for the presented new-typed OAM horn antenna.

1. INTRODUCTION

Vortex wave is a type of electromagnetic(EM) wave carrying orbital angular momentum(OAM) [1], and its phase wavefront is no longer a plane, but rotates around the direction of propagation, with twisted structure [2]. The phase rotation factor $e^{-jl\varphi}$ [3] determines the spatial phase distribution structure of the vortex beam, in which l represents the mode of the orbital angular momentum. Moreover, the OAM beams with different modes are mutually orthogonal and have different spatial structures. Therefore, the OAM EM wave is considered to improve the spectral utilization by modulating the multipath signal to different orbital angular momentum modes [4].

In recent years, a lot of antenna designs have been proposed to generate OAM EM waves, which can be divided into two categories. The first one is asymmetric physical structure or feed structure, such as the modified spiral paraboloid antenna [5], stepped reflector antenna [6], spiral phase plate [7], horn antenna with SPP [8], elliptical microstrip antenna [9], spiral antenna [10]. Among them, antennas in [5–8] with spiral structure on azimuth φ which result in the phase delay of the reflected wave or the transmitted wave, thus the orbital angular momentum is obtained. In the article [9, 10], the asymmetric structure of antennas lead to the asymmetry of the radiation field. The second is to create phase difference using multi-point feeding, such as the circular patch antenna [11], circular antenna array [12–16], the half mode substrate integrated waveguide antenna [17], etc. Antennas in [11, 17] fed with two same signals but with a $\pi/2$ phase shift to get phase factor $e^{-jl\varphi}$. Antennas in n elements circular antenna array of [12–16] are fed with same amplitude and a progressive $2\pi l/n$ phase shift signals in order to get $2\pi l$ phase delay. However, antennas in the first type are restricted to a single OAM mode, and most of them only can generate the first-order OAM. The structures of second type are complex, especially the complicated feed network of the circular antenna array.

On the contrary, this paper presents a rather simple method (has been briefly introduced in paper [18]) to generate orbital angular momentum electromagnetic wave using horn antenna. In order to demonstrate the feasibility of this method, a design based on TE_{21} mode to generate an OAM with order $\pm m$ and $\pm(m-1)$ is presented.

Received 8 March 2017, Accepted 10 May 2017, Scheduled 29 August 2017

* Corresponding author: Min Huang (huangmin@std.uestc.edu.cn).
The authors are with Department of Microwave Engineering, University of Electronic Science and Technology of China, Chengdu, Sichuan 610054, China.

2. THEORETICAL ANALYSIS

The structure of a circular waveguide has a high degree of axial symmetry, and the expressions of each field component of TE_{mn} $(m \neq 0)$ mode in the waveguide are

$$\begin{aligned} E_z &= 0 \\ E_r &= \pm j\frac{\omega\mu m}{K_c^2 r} H_0 J_m(K_c r)^{\sin(m\varphi)}_{\cos(m\varphi)} e^{-j\beta z} \\ E_\varphi &= j\frac{\omega\mu}{K_c} H_0 J_m'(K_c r)^{\cos(m\varphi)}_{\sin(m\varphi)} e^{-j\beta z} \end{aligned} \tag{1}$$

where r is the radius of the waveguide, K_c the cutoff wavenumber, J_m the m-order Bessel function, J_m' the derived function of m-order Bessel function, φ the azimuth, and m the mode number of circular waveguide.

From the expressions above, the x and y components can be expressed as:

$$E_x = E_r\cos\varphi - E_\varphi \sin\varphi = \pm\frac{1}{2}(A-B)^{\sin(m+1)\varphi}_{\cos(m+1)\varphi} \pm (A+B)^{\sin(m-1)\varphi}_{\cos(m-1)\varphi} \tag{2}$$

$$E_y = E_r\sin\varphi + E_\varphi \cos\varphi = -\frac{1}{2}(A-B)^{\cos(m+1)\varphi}_{\sin(m+1)\varphi} + \frac{1}{2}(A+B)^{\cos(m-1)\varphi}_{\sin(m-1)\varphi} \tag{3}$$

where

$$\begin{aligned} A &= j\frac{\omega\mu m}{K_c^2 r} H_0 J_m(K_c r) e^{-j\beta z} \\ B &= j\frac{\omega\mu}{K_c} H_0 J_m'(K_c r) e^{-j\beta z} \end{aligned} \tag{4}$$

The ratio of $(A+B)/(A-B)$ is shown in Fig. 1, and it is obvious that $(A+B)$ is significantly bigger than $(A-B)$ (the dominant position of $(A+B)$ is also reflected in the phase diagram of Fig. 4), and Equations (2) and (3) can be written as:

$$\begin{aligned} E_x &\approx \pm\frac{1}{2} H_0 \left[j\frac{\omega\mu m}{K_c^2 r} J_m(K_c r) + j\frac{\omega\mu}{K_c} J_m'(K_c r) \right]^{\sin(m-1)\varphi}_{\cos(m-1)\varphi} e^{-j\beta z} \\ E_y &\approx \frac{1}{2} H_0 \left[j\frac{\omega\mu m}{K_c^2 r} J_m(K_c r) + j\frac{\omega\mu}{K_c} J_m'(K_c r) \right]^{\cos(m-1)\varphi}_{\sin(m-1)\varphi} e^{-j\beta z} \end{aligned} \tag{5}$$

Due to the symmetry of circular waveguide, there are two possible distributions of the field expressions along φ: $\sin(m\varphi)$ and $\cos(m\varphi)$. The field structures of two distributions are exactly the same, except

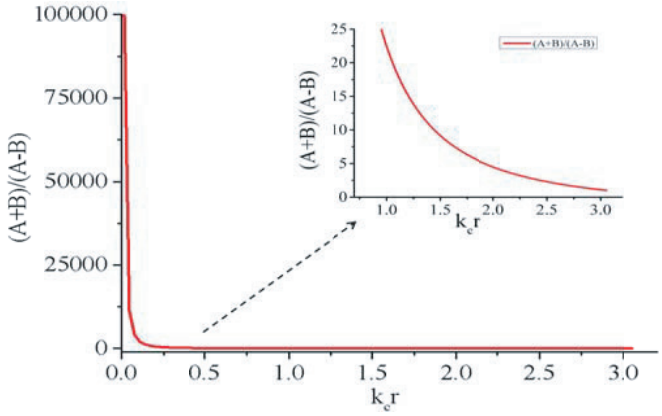

Figure 1. Ratio between the terms $(A+B)$ and $(A-B)$.

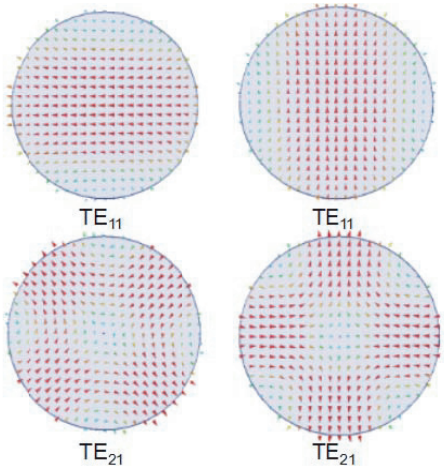

Figure 2. Electric field distribution in circular waveguide.

the direction of polarization with a 90°-phase difference, which is the special polarization degenerate characteristic in the circular waveguide, as shown in Fig. 2. Therefore, the required phase factor can be obtained by combining two orthogonal polarization degenerate TE_{mn} modes (Here m is equivalent to l, which refers to orbital angular momentum orders, and is a non-zero integer).

$$\begin{aligned} &TE_{mn} \pm jTE_{mn}: \\ &E_r(r,\varphi,z) = \pm j\frac{\omega\mu m}{K_c^2}H_0 J_m(K_c r)e^{\pm jm\varphi}e^{-j\beta z} \\ &E_\varphi(r,\varphi,z) = j\frac{\omega\mu}{K_c}H_0 J'_m(K_c r)e^{\pm jm\varphi}e^{-j\beta z} \end{aligned} \tag{6}$$

$$\begin{aligned} E_x &\approx \pm\frac{1}{2}H_0\left[j\frac{\omega\mu m}{K_c^2}J_m(K_c r) + j\frac{\omega\mu}{K_c}J'_m(K_c r)\right]e^{\pm j(m-1)\varphi}e^{-j\beta z} \\ E_y &\approx \frac{1}{2}H_0\left[j\frac{\omega\mu m}{K_c^2}J_m(K_c r) + j\frac{\omega\mu}{K_c}J'_m(K_c r)\right]e^{\pm j(m-1)\varphi}e^{-j\beta z} \end{aligned} \tag{7}$$

It is obvious from Expressions (6) and (7) that the field components of r and φ contain the phase rotation factor $e^{\pm jm\varphi}$, and components of x and y have the phase rotation factor $e^{\pm j(m-1)\varphi}$. In order to verify the analysis above, TE_{11}, TE_{21} and TE_{31} modes of circular waveguide are simulated in HFSS to observe the phase distribution of different field components. As shown in Fig. 3 and Fig. 4, the phase

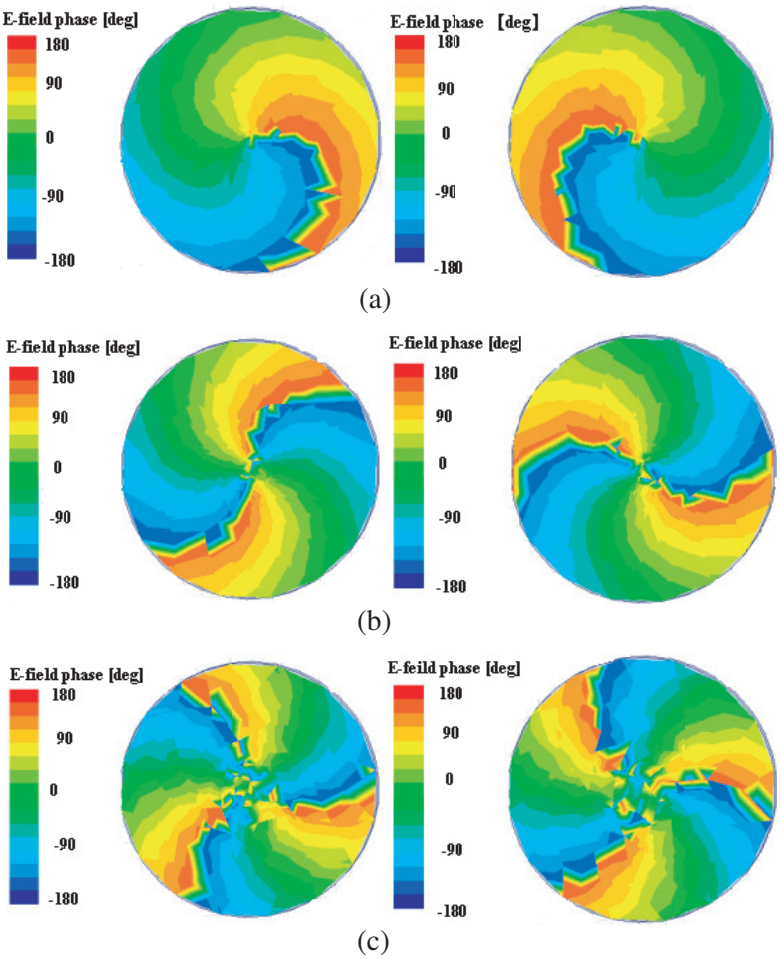

Figure 3. Phase patterns of r components of electric field. (a) Two orthogonal TE_{11} modes; (b)two orthogonal TE_{21} modes; (c) two orthogonal TE_{31} modes.

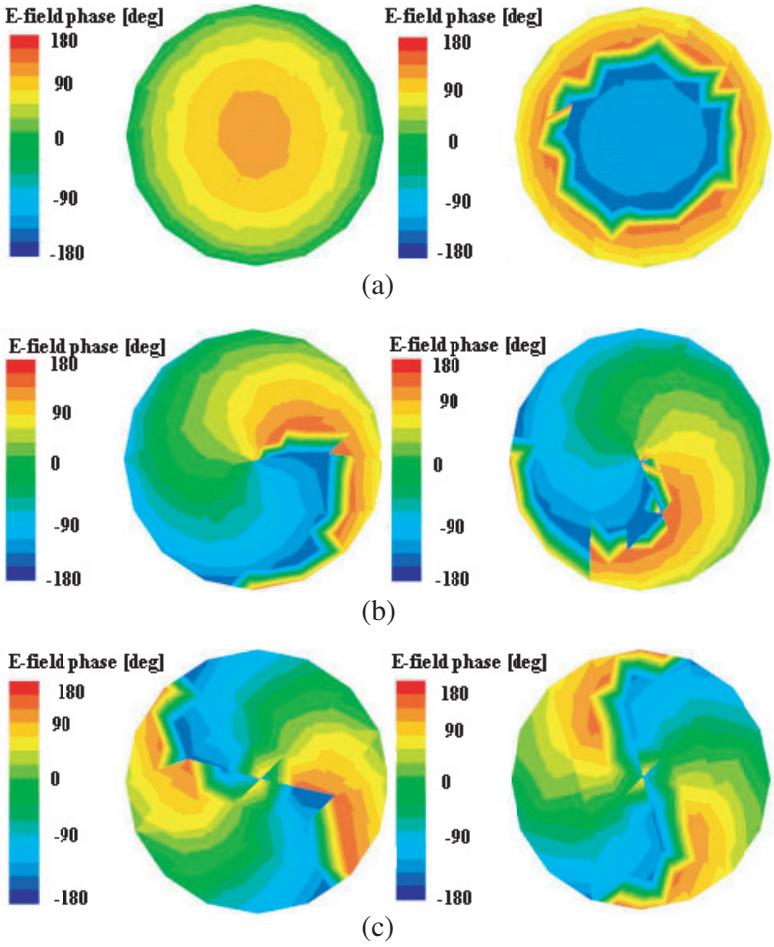

Figure 4. Phase patterns of x (left) and y (right) components of the electric field. (a) Two orthogonal TE_{11} modes; (b) two orthogonal TE_{21} modes; (c) two orthogonal TE_{31} modes.

changes of r and φ components are $2m\pi$, and on the contrary, the phase changes of x and y components are $2(m-1)\pi$.

3. ANTENNA DESIGN AND SIMULATION

In the previous section, the theory of the orbital angular momentum generated by the circular waveguide is described. In order to verify the theory, an antenna worked at 9.2 GHz is presented. The detailed dimensions of the antenna are marked in Fig. 5. The antenna is composed of three sections. The first section is the main mode excitation section of circular waveguide, the radius of which satisfies the transmission condition of the main mode:

$$\begin{gathered} \lambda_{cTM01} < \lambda < \lambda_{cTE_{11}} \\ \lambda_c = \frac{2\pi r}{\mu_{mn}} \\ \lambda = c/f \\ 9.56\,\text{mm} < r < 12.49\,\text{mm} \end{gathered} \tag{8}$$

In Formula (8), λ_c is the cutoff wavelength and μ_{mn} the root of Bessel function. The second section is the transition section, and the radius of the cone gradually varies from the single mode transmission condition to TE_{21} mode transmission condition, which satisfies the transmission condition of the TE_{21}

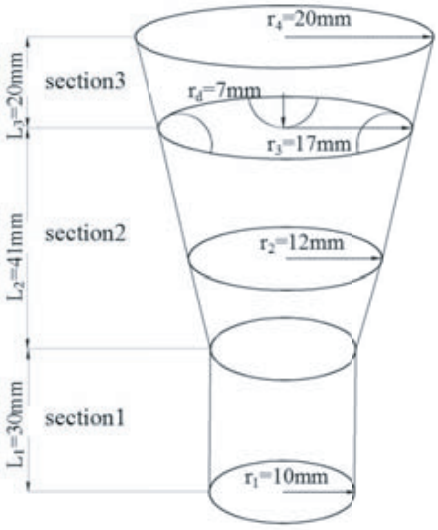

Figure 5. Schematic diagram of antenna.

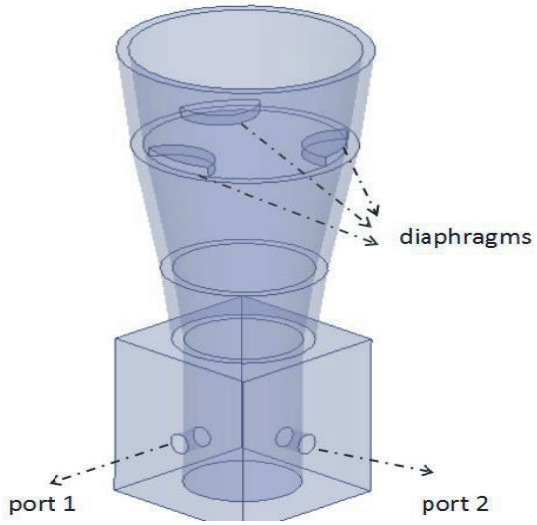

Figure 6. Antenna simulation model.

mode:

$$\begin{gathered}\lambda_{cTM_{01}} < \lambda < \lambda_{cTE_{21}} \\ 15.83\,\text{mm} < r < 19.88\,\text{mm}\end{gathered} \tag{9}$$

The third section is the mode transition section where the main mode will be converted to TE21 mode by diaphragm perturbation.

Therefore, in the first section, $r_1 = 10\,\text{mm}$, only the main mode of the waveguide can be excited and spread. In the second section, $r_2 = 12\,\text{mm}$, so that the main mode can be adequately spread. In the third section, $r_3 = 17\,\text{mm}$, the TE_{21} mode can be formed by the perturbation of the three pieces of metal. The length of each section and dimension of the metal diaphragm are selected to make sure that antenna is well matched at 9.2 GHz.

An example of a horn antenna in HFSS, which can generate orbital angular momentum beam of order 2 or -2, and 1 or -1, is shown in Fig. 6. The circular waveguide section at the bottom of the antenna has two excitation ports, and these two ports are arranged with a 90-degree angle on the circumference and fed by coaxial cables. The output frequencies and amplitudes of these two sources are the same, except the 90-degree phase difference, which is used to excite two orthogonal polarization modes. The 90° or −90° of the feed phase difference determines the positive or negative of the OAM order, that is, the phase pattern rotation is clockwise or anticlockwise. As shown in Fig. 7, the three diaphragms have the same size and are spaced 120 degrees, which are used to disturb the electric field

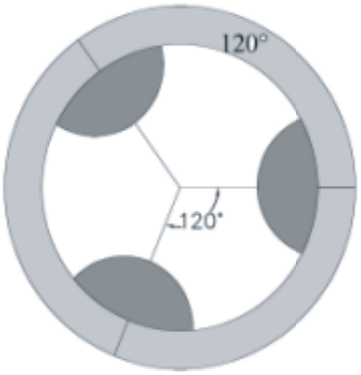

Figure 7. Distribution metal diaphragms.

distribution of the main mode, thus forming the TE_{21} mode.

The phase patterns of the proposed structure have been simulated by FEKO. The phase patterns of r and φ components of the radiated electric field are shown in Fig.8, and x and y components are shown in Fig. 9. The phase patterns are calculated at a 20λ distance from the horn aperture. It is apparent that the phase patterns of r and φ components have a clockwise or anticlockwise rotation with a 4π phase change, which corresponds to the phase factor of $e^{\pm j2\varphi}$, and the phase patterns of x and y components have the same rotation direction but with a 2π phase change, which corresponds to the phase factor of $e^{\pm j\varphi}$.

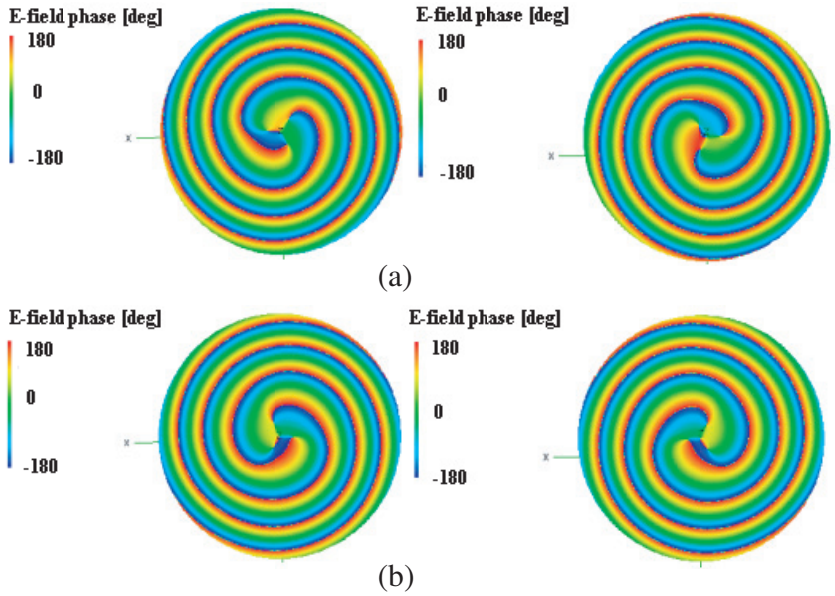

Figure 8. Phase patterns at 9.2 GHz. (a) φ component of the electric field; (b) r component of the electric field.

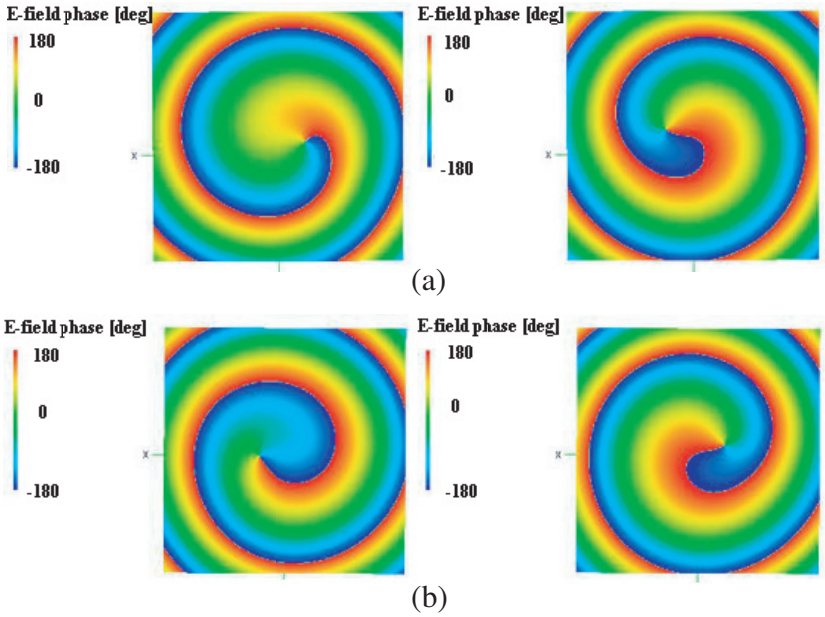

Figure 9. Phase patterns at 9.2 GHz. (a) x component of the electric field; (b) y component of the electric field.

4. MEASUREMENTS

The proposed horn antenna with the specific structure shown in Fig. 6 is fabricated. Two SMA connectors are used to feed the horn, as shown in Fig. 10. The phase patterns are measured in a microwave anechoic chamber. The phase pattern results of x component measured at 20λ distance from the horn aperture are shown in Fig. 11. Obvious spiral phase distribution corresponding to OAM of order -1 can be observed in the figure, which is well consistent with the simulation result in Fig. 9. The measured amplitude distribution is shown in Fig. 12, and the minimum amplitude corresponds to the vortex center, which is the characteristic of the vortex beam.

Figure 10. Photograph of conical horn antenna.

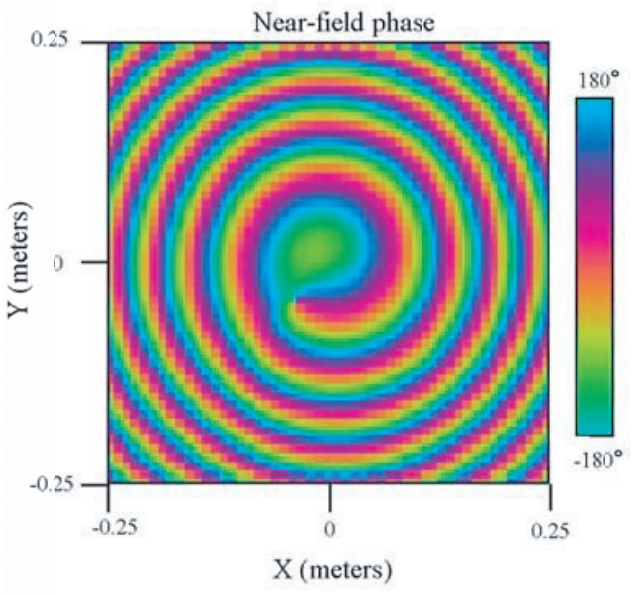

Figure 11. Measured x component radiation phase pattern.

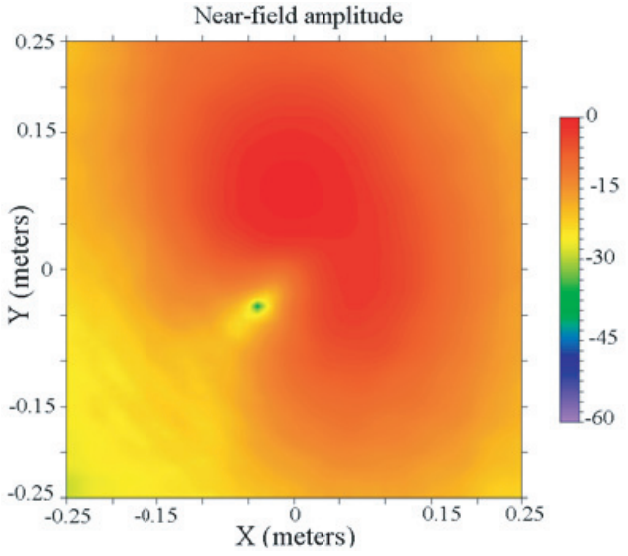

Figure 12. Measured x component radiation amplitude distribution.

5. CONCLUSION

A novel method and a simple antenna design for generating radio OAM waves are proposed in this paper. Both the theoretical analysis and experiment results are presented. Based on TE_{21} mode of the circular waveguide, the OAM with mode of $l = 2$ or $l = -2$ is generated for E_r and E_φ components, $l = 1$ or $l = -1$ for E_x and E_y components, respectively. The measured phase patterns of electrical field components are consistent with the simulation results. In conclusion, with a proper design, circular waveguide can generate OAM electromagnetic field of order $\pm m$ and $\pm(m-1)$. In addition, compared with other forms of OAM antenna already published, the antenna designed in this paper is simpler, easier to process and can realize two modes simultaneously.

ACKNOWLEDGMENT

This work is supported by the National Natural Science Foundation of China (NSFC) under Project Nos. 61401063 and 61231001.

REFERENCES

1. Cohen-Tannoudji, C., J Dupont-Roc, and G. Grynberg, *Chapter 5. Introduction to the Covariant Formulation of Quantum Electrodynamics. Photons and Atoms: Introduction to Quantum Electrodynamics*, 361–455, Wiley-VCH Verlag GmbH, 2007.
2. Poynting, J. H., "The wave motion of a revolving shaft, and a suggestion as to the angular momentum in a beam of circularly polarised light," *Proceedings of the Royal Society A*, Vol. 82, No. 557, 560–567, 1909.
3. Thidé, B., H. Then, J. Sjöholm, et al., "Utilization of photon orbital angular momentum in the low-frequency radio domain," *Physical Review Letters*, Vol. 99, No. 8, 2007.
4. Gibson, G., J. Courtial, M. Padgett, et al., "Free-space information transfer using light beams carrying orbital angular momentum," *Optics Express*, Vol. 12, No. 22, 5448–5456, 2004.
5. Tamburini, F., E. Mari, A. Sponselli, et al., "Encoding many channels in the same frequency through radio vorticity: First experimental test," *New J. Phys.*, Vol. 14, No. 3, 811–815, 2013.
6. Tamburini, F., E. Mari, B. Thide, et al., "Experimental verification of photon angular momentum and vorticity with radio techniques," *Applied Physics Letters*, Vol. 99, No. 20, 321, 2011.
7. Bennis, A., R. Niemiec, C. Brousseau, et al., "Flat plate for OAM generation in the millimeter band," *European Conference on Antennas and Propagation*, 3203–3207, 2013.
8. Wei, W., K. Mahdjoubi, C. Brousseau, et al., "Horn antennas for generating radio waves bearing orbital angular momentum by using spiral phase plate," *Iet Microwaves Antennas & Propagation*, 10, 2016.
9. Barbuto, M., A. Toscano, and F. Bilotti, "Single patch antenna generating electromagnetic field with orbital angular momentum," *IEEE International Symposium on Antennas and Propagation & USNC/URSI National Radio Science Meeting*, 1866–1867, IEEE, 2013.
10. Al-Bassam, A., M. A. Salem, and C. Caloz, "Vortex beam generation using circular leaky-wave antenna," *Antennas and Propagation Society International Symposium*, 1792–1793, IEEE, 2014.
11. Barbuto, M., F. Trotta, F. Bilotti, and A. Toscano, "Circular polarized patch antenna generating orbital angular momentum" *Progress In Electromagnetics Research*, Vol. 148, 23–30, 2014.
12. Thidé, B., H. Then, J. Sjöholm, et al., "Utilization of photon orbital angular momentum in the low-frequency radio domain," *Physical Review Letters*, Vol. 99, No. 8, 087701, 2007.
13. Mohammadi, S. M., L. K. S. Daldorff, and J. E. S. Bergman, "Orbital angular momentum in radio — A system study," *IEEE Transactions on Antennas & Propagation*, Vol. 58, No. 2, 565–572, 2010.
14. Wu, H., Y. Yuan, and Z. Zhang, "UCA-based orbital angular momentum radio beam generation and reception under different array configurations," *Sixth International Conference on Wireless Communications and Signal Processing*, 1–6, IEEE, 2014.

15. Tennant, A. and B. Allen, "Generation of OAM radio waves using circular time-switched array antenna," *Electronics Letters*, Vol. 48, No. 21, 1365–1366, 2012.
16. Bai, Q., A. Tennant, and B. Allen, "Experimental circular phased array for generating OAM radio beams," *Electronics Letters*, Vol. 50, No. 20, 1414–1415, 2014.
17. Chen, Y. L., S. L. Zheng, and H. Chi, "Orbital angular momentum mode multiplexing antenna based on half mode substrate integrated waveguide," *National Conference on Microwave and Millimeter Waves*, 2015.
18. Huang, M., X. Z. Zong, and Z. P. Nie, "Method to generate electromagnetic field with orbital angular momentum in circular waveguide," *IEEE International Symposium on Antennas and Propagation & USNC/URSI National Radio Science Meeting*, 1897–1898, Puerto Rico, 2016.